EUROPEAN ORGANIZATION FOR NUCLEAR RESEARCH

CERN–PPE/94–177
21 November 1994

Directional dependence of the pion source in high-energy heavy-ion collisions

H. Bøggild[1], J. Boissevain[2], M. Cherney[3], J. Dodd[4], S. Esumi[5], C.W. Fabjan[6], D. E. Fields[2], A. Franz[6], K.H. Hansen[1], B. Holzer[6], T. J. Humanic[7], B.V. Jacak[2], R. Jayanti[7,8], H. Kalechofsky[8,a], T. Kobayashi[9,b], R. Kvatadze[6,c], Y.Y. Lee[8,d], M. Leltchouk[4], B. Lörstad[10], N. Maeda[5], A. Medvedev[4], Y. Miake[11,e], A. Miyabayashi[10], M. Murray[12], S. Nishimura[5], E. Noteboom[3], S.U. Pandey[7], F. Piuz[6], V. Polychronakos[11], M. Potekhin[4], G. Poulard[6], A. Sakaguchi[5], M. Sarabura[2], M. Spegel[6], K. Shigaki[9,f], J. Simon-Gillo[2], W. Sondheim[2], T. Sugitate[5], J. P. Sullivan[2], Y. Sumi[5], H. van Hecke[2], W.J. Willis[4] and K.Wolf[12]

Abstract

$\pi^+\pi^+$ and $\pi^-\pi^-$ correlations from 200 GeV per nucleon S + Pb collisions and $\pi^+\pi^+$ correlations from 450 GeV p + Pb collisions measured by the focusing spectrometer of CERN experiment NA44 are presented. The large data set which emphasizes small values of momentum difference allows multi-dimensional analysis along with the more traditional one-dimensional parameterization to characterize the pion emission source. It is found that the three radius parameters are similar and large compared to the projectile radius. This can be explained by pion scattering in the final state hadronic system.

(To Be Submitted to Physics Letters B.)

[1] Niels Bohr Institute, DK-2100 Copenhagen, Denmark.
[2] Los Alamos National Laboratory, Los Alamos, NM 87545, USA.
[3] Creighton University, Omaha, NE 68178, USA.
[4] Columbia University, New York, NY 10027, USA.
[5] Hiroshima University, Higashi-Hiroshima 724, Japan.
[6] CERN, CH-1211 Geneva 23, Switzerland.
[7] Ohio State University, Columbus, OH 43210, USA
[8] University of Pittsburgh, Pittsburgh, PA 15260, USA.
[9] National Laboratory for High Energy Physics, Tsukuba 305, Japan.
[10] University of Lund, S-22362 Lund, Sweden.
[11] Brookhaven National Laboratory, Upton, NY 11973, USA.
[12] Texas A&M University, College Station, TX 77843, USA.
[a] Now at University of Geneva.
[b] Now at Riken Linac Laboratory, Riken, Saitama 351-01, Japan.
[c] Visitor from Tbilisi State University, Tbilisi, Rep. of Georgia.
[d] Now at GSI Laboratory, Darmstadt, Germany.
[e] Now at Tsukuba University, Tsukuba 305, Japan.
[f] University of Tokyo, Tokyo 113, Japan.

1 INTRODUCTION

Two-particle intensity interferometry can provide information on the space–time extent of the particle-emitting source [1, 2, 3, 4], and shed light on the dynamical evolution of heavy-ion collisions. In particular, intensity interferometry provides information on the time span of particle emission, which in the case of a first order phase transition in a QGP can be long compared to the equivalent spatial extent of the source [5, 10]. Such studies require good momentum resolution and high statistics, especially at small momentum differences.

NA44 is optimized for the study of identified single- and two-particle distributions at mid-rapidity. The spectrometer is a focusing spectrometer, a design which optimizes the acceptance for pairs of particles with small momentum difference. This allows small statistical uncertainties in the two-particle correlation function in the region of the signal from Bose–Einstein correlations. We present the study of three components of the momentum difference which are sensitive to the space–time character of the collision dynamics. Results from the one-dimensional analysis are also presented in order to make comparisons with other experiments and to observe trends in data sets.

2 THE EXPERIMENTAL SET-UP

The focusing spectrometer of the NA44 experiment has been described in detail elsewhere [7]. Two dipole magnets and three quadrupoles create a magnified image of the target in the spectrometer. Only one charge sign can be detected in the spectrometer at a time. The momentum range selected in this analysis covers a band of $\pm$ 20% around the nominal momentum setting of 4 GeV/c. The beam rate and time-of-flight start signal for the sulphur beam are determined using a Cherenkov beam counter with time resolution of approximately 35 ps [8]; for the proton beam a scintillator interaction counter is used. A silicon pad detector is used to measure the charged-particle multiplicity distribution with 2π azimuthal acceptance in the pseudorapidity range $1.8 < \eta < 3.3$.

The spectrometer uses three highly segmented scintillator hodoscopes [9] for tracking and time-of-flight measurements. In this analysis we use the time measured between the last hodoscope and the start counter for time-of-flight with total resolution $\approx$ 100 ps. Together with the two gas Cherenkov counters this provides good particle identification.

3 DATA ANALYSIS

Two spectrometer settings are needed to optimize the acceptance and resolution. The 'horizontal' spectrometer setting optimizes the acceptance in p_x and p_z while the 'vertical' setting optimizes the acceptance in p_y and p_z, where z is along the incident beam. The pair statistics for various data sets are listed in Table 1.

Data	Horizontal	Vertical
S + Pb $\rightarrow \pi^+\pi^+ + X$	114,000	87,000
S + Pb $\rightarrow \pi^-\pi^- + X$	60,000	–
p + Pb $\rightarrow \pi^+\pi^+ + X$	160,000	132,000

Table 1: Pair Statistics for various Data sets.

The single-particle acceptance curves for both the horizontal and vertical settings are shown in Figs. 1a and 1b. The rapidity range spanned is 3.2 to 4.2 and the p_T range covered is from 0.0 to 0.6 GeV/c. For the sulphur beam at 200 GeV per nucleon the lead

target was 2 mm thick while for the proton beam at 450 GeV the target was 10 mm lead. The most central 3% of the events have been selected based on Si counter multiplicity information. Particles are identified based on the Cherenkov signal and the mass spectrum constructed from momentum and time-of-flight. Fig. 1c shows the measured mass-squared distribution. Contamination of $\pi\pi$ events by π K and other particles such as electrons, which are rejected by the second Cherenkov counter, is less than 1%.

The raw correlation function is determined using

$$C_{raw}(\vec{k_1},\vec{k_2}) = \frac{R(\vec{k_1},\vec{k_2})}{B(\vec{k_1},\vec{k_2})}\,, \tag{1}$$

where $\vec{k_i}$ are the particle momenta. The 'real distribution' $R(\vec{k_1},\vec{k_2})$ is the distribution of the relative momentum in an event. The 'background distribution' $B(\vec{k_1},\vec{k_2})$ is generated as follows: for each event in $R(\vec{k_1},\vec{k_2})$, ten pairs of events are selected randomly to form the background pairs. In these pairs, one particle in each event is selected randomly to create a new 'event' for the $B(\vec{k_1},\vec{k_2})$ distribution. As in the real distribution, events from $B(\vec{k_1},\vec{k_2})$ are subjected to the same analysis procedures. Distortions of the correlation function due to final state Coulomb interactions [6], residual background corrections [11, 12] and momentum smearing are treated as in [7].

The measured two-particle correlation is related to the true correlation by

$$C_{corr}(\vec{k_1},\vec{k_2}) = C_{raw}(\vec{k_1},\vec{k_2}) \times K_{SPC}(\vec{k_1},\vec{k_2}) \times K_{acceptance}(\vec{k_1},\vec{k_2})\,, \tag{2}$$

where $K_{SPC}(\vec{k_1},\vec{k_2})$ corrects for the distortion of the single-particle spectrum due to residual correlations, $K_{acceptance}(\vec{k_1},\vec{k_2})$ is the correction for the distortion of the two-particle spectrum by the momentum resolution and the two-particle acceptance of the detectors and K_{coul} corrects for the final state Coulomb interactions. All three corrections, K_{SPC}, $K_{acceptance}$ and K_{coul}, depend on the source size and the fitting results, so an iterative approach is required [7]. We do not consider screening effects due to particles of opposite charge in a high-particle-density environment. Such effects are believed to have only a small influence on the Coulomb correction [13, 14].

We use the following fit functions:

$$C(Q_{inv}) = A(1+\lambda e^{-Q_{inv}^2 R_{inv}^2}); \quad Q_{inv} = \sqrt{Q^2 - Q_0^2} \tag{3}$$

$$C(Q_{R=\tau}) = A(1+\lambda e^{-Q_{R=\tau}^2 R_{R=\tau}^2}); \quad Q_{R=\tau} = \sqrt{Q^2 + Q_0^2} \tag{4}$$

and

$$C(Q_{t_o},Q_{t_s},Q_l) = A(1+\lambda e^{-Q_{t_o}^2 R_{t_o}^2 - Q_{t_s}^2 R_{t_s}^2 - Q_l^2 R_l^2}) \tag{5}$$

Where

$$Q = |\vec{p_1} - \vec{p_2}|,\ Q_0 = |E_1 - E_2| \tag{6}$$

Fits in one dimension using either Q_{inv} or $Q_{R=\tau}$ inherently assume a spherical source. The interpretation of extracted parameters from the fits to Q_{inv} or $Q_{R=\tau}$ are influenced by Lorentz effects which vary for different particle species [15]. Our data permit analysis in three dimensions and enable better interpretation of the extracted parameters. The momentum difference of the particle pair is resolved into Q_l parallel to the beam and Q_T perpendicular to the beam direction. Q_T is further resolved into a component Q_{t_o} parallel

to the pair momentum sum and Q_{t_s} perpendicular to the transverse pair momentum sum. Being parallel to the velocities of the particles, Q_{t_o} is sensitive to the lifetime of the source [13]. The data are analyzed in the frame in which the z-component ($p_z = p_{z_1} + p_{z_2}$) of the pair momentum sum is zero. In this frame the lifetime information is coupled only to Q_{t_o}.

The three-dimensional fits require data from both the horizontal and vertical spectrometer settings. Bin sizes of 10 MeV/c have been used in this analysis. No bins were excluded while fitting. Systematic errors on the fit parameters are estimated by reanalyzing the data under two altered conditions. The conditions varied are: (*i*) rejecting tracks which hit neighbouring slats on *all* three hodoscopes and (*ii*) degrading the momentum resolution by 10% (estimated maximum uncertainty). The estimated systematic errors thus obtained are approximately equal to the statistical errors. Further details of the systematic error analysis can be found elsewhere [16].

4 Results and Discussion

Fits to Q_{t_s}, Q_{t_o} and Q_l are performed on the S + Pb and p + Pb data sets; the results for the three-dimensional fits from the horizontal and vertical spectrometer setting are summarized in Table 2 and shown together with the data in Figure 2. The R parameters increase from p+Pb collisions to S+Pb collisions and are larger than the corresponding R parameters from the kaon pairs for similar systems [7]. These trends are supported by source parameters extracted from Q_{inv} and $Q_{R=\tau}$ shown in Table 3 and Table 4. The radius parameters from the R = τ fit for $\pi^+\pi^+$ and $\pi^-\pi^-$ are similar, indicating that the Coulomb effects from excess charged particles such as protons are not significant in S + Pb collisions. This trend is supported by the single-particle spectra of π^+ and π^-, which are found to be very similar [17].

Our three-dimensional analysis of p+Pb and S+Pb data indicates that within rather small errors

$$R_{t_s} \approx R_{t_o} \approx R_l \ . \tag{7}$$

These results may be interpreted in the following way: (*i*) a first order phase transition, which would lead to R_{t_o} significantly larger than R_{t_s} [5, 10], is not borne out in our results; (*ii*) the lifetime parameter, τ,which represents the width of freezeout time distribution, is estimated from the static Gaussian model as

$$\tau = 1/\beta\sqrt{R_{t_o}^2 - R_{t_s}^2} \tag{8}$$

where β is the average transverse velocity of the particle pair; we find that this time is rather short, i.e. less than a few fermi/c.

It is instructive to compare our measured R_{t_s} parameter to the radius of the projectile nucleus. The equivalent Gaussian radius is given by:

$$R_{gauss} = 1.2A^{1/3}/\sqrt{5}\ \ fm \tag{9}$$

where A is the number of nucleons. The R_{gauss} for sulphur and proton are 1.69 fm and 0.44 fm respectively, both of which are considerably smaller than the measured R_{t_s}. This indicates considerable expansion of the source before freezeout.

Some light can be shed on the above observations by comparison with the microscopic simulation, RQMD, with which the space-time history of the particles can be calculated. Figure 4 shows comparison of our experimental correlation functions with

RQMD [18, 19, 20] for the S + Pb system. Reasonable agreement is seen with the data. The R_{t_s} and R_{t_o} parameters extracted from RQMD are also seen to be similar.

Furthermore, it is possible to relate the space–time history of particles at freeze-out to the R parameters, including effects such as rescattering, resonance decays and acceptance of the experiment. This model can also be used for the physical interpretation of the extracted fit parameters which are different from the actual radius and lifetime of the source due to correlations between the particles' momentum and position. These correlations are induced by the expansion of the source driven by particle rescattering [21].

Our RQMD calculations of R_{t_s}, which most closely reflects the transverse source size, yield 4.7 ± 0.4 fm. This value is consistent with the measured $R_{t_s} = 4.15 \pm 0.27$ fm. We can also evaluate the RMS freezeout radius with RQMD by fitting a Gaussian directly to the particle position distribution at freezeout. For the y-p_T region of our measurements, the RQMD calculated RMS freezeout radius is 3.4 fm. This radius is considerably smaller than the R_{t_s}. We can also evaluate with RQMD the lifetime parameter τ by fitting a Gaussian directly to the particle freezeout time distribution. The width of the freezeout time distribution is calculated to be $\approx 5\text{fm}/c$. The differences between the HBT extracted parameters, R_{t_S} and τ from eq. 8, and the actual source parameters, the RMS freeze-out radius and τ from RQMD, can be quantitatively understood as a consequence of momentum-position correlations [20].

Other experimental evidence[22, 16, 23, 24] is also consistent with our interpretation of an expanding system. Data obtained at lower energies at the AGS [15] indicate smaller R parameters. This may reflect the smaller number of particles produced at the lower energies, resulting in less secondary scattering after creation and consequently less source expansion.

5 CONCLUSIONS

The striking predictions of a possible phase transition are not seen in our data. The R_{t_s} and R_{t_o} parameters are similar. The radius parameters extracted for pions is larger than that of the kaons for similar systems, which could be attributed to resonance decays and rescattering in the source before freezeout. The radii we measure both for S + Pb and p + Pb are larger than the projectile, indicating that there is an expansion of the hadronic final state, in agreement with the fact that the radius parameters we measure are larger compared to the lower energy data.

6 ACKNOWLEDGEMENTS

The NA44 Collaboration wishes to thank the staff of the CERN PS-SPS accelerator complex for their excellent work. We thank the technical staff at CERN and the collaborating institutes for their valuable contribution. We are also grateful for the support given by the W. M. Keck foundation; the Österreichische Fond zur Förderung der Wissenschaftlichen Forschung; the Science Research Council of Denmark; the Japanese Society for the Promotion of Science, and the Ministry of Education, Science and Culture, Japan; the Science Research Council of Sweden; the US Department of Energy; and the National Science Foundation.

References

[1] R. Hanbury-Brown and R. Q. Twiss, *Nature* **178** (1956) p. 1046.
[2] G. Goldhaber *et al.*, *Phys. Rev.* **120** (1960) p. 300.
[3] M. Gyulassy and S.K. Kauffmann and L.W. Wilson, *Phys. Rev.* **C20** (1979) p. 2267.
[4] B. Lorstad, *Mod. Phys.* **A4** (1989) p. 2861.
[5] G. Bertsch and G.E. Brown, *Phys. Rev.* **C40** (1989) p. 1830.
[6] S. Pratt, *Phys. Rev.* **D33** (1986) p. 1314.
[7] H. Becker *et al.*, *Phys. Lett.* **B302** (1993) p. 510.
[8] N. Maeda *et al.*, *Nucl. Meth. Instr.* **A346** (1994) p. 132.
[9] T. Kobayashi and T. Sugitate, *Nucl. Inst. Meth.* **A287** (1990) p. 389.
[10] S. Pratt, *Phys. Rev.* **D33** (1986) p. 72.
[11] W.A. Zajc *et al.*, *Phys. Rev.* **C29** (1984) p. 2173.
[12] K. Kadija, *Phys. Lett.* **B287** (1992) p. 362.
[13] S. Pratt and T. Csörgő and J. Zimányi, *Phys. Rev.* **C42** (1990) p. 2646.
[14] M.G. Bowler, *Z. Phys.* **C46** (1990) p. 305.
[15] Y. Akiba *et al.*, *Phys. Rev. Lett.* **70** (1993) p. 1057.
[16] H. Beker *et al.*, CERN–PPE/94–75 and *Z. Phys.* (in press) (1994).
[17] H. Beker *et al.*, Low p_T phenomeanon in pA and AA collisions at mid-rapidity, 1994, to be published.
[18] H. Sorge and H. Stöcker and W. Greiner, *Nucl. Phys.* **A498** (1989) p. 567.
[19] J.P. Sullivan *et al.*, *Phys. Rev. Lett.* **70** (1993) p. 3000.
[20] D.E. Fields *et al.*, 1994, to be published.
[21] T.J. Humanic, *Phys. Rev. C* (in press) **C50** (1994).
[22] H. Beker *et al.*, CERN–PPE/94–119 and submitted to *Phys. Rev. Lett.* (1994).
[23] T. Alber *et al.*, IKF–HENPG/9–94 (1994).
[24] T. Alber *et al.*, submitted to *Phys. Rev. Lett.* LBL–36062 (1994).

Data	λ	R_{ts}	R_{to}	R_l	χ^2/DOF
S + Pb $\rightarrow \pi^+\pi^+ + X$	0.56 ± 0.02	4.15 ± 0.27	4.02 ± 0.14	4.73 ± 0.26	1201/1415
p + Pb $\rightarrow \pi^+\pi^+ + X$	0.41 ± 0.02	2.00 ± 0.25	1.92 ± 0.13	2.34 ± 0.36	1111/1152

Table 2: Result of Gaussian parametrizations in Q_{t_s}, Q_{t_o} and Q_l

Data	λ	R_{inv}	χ^2/DOF
S + Pb $\rightarrow \pi^+\pi^+ + X$	0.56 ± 0.03	5.00 ± 0.22	29/25
S + Pb $\rightarrow \pi^-\pi^- + X$	0.42 ± 0.02	4.00 ± 0.27	19/25
p + Pb $\rightarrow \pi^+\pi^+ + X$	0.38 ± 0.03	2.89 ± 0.30	16/25

Table 3: Result of Gaussian parametrizations in Q_{inv}

Data	λ	$R_{r=\tau}$	χ^2/DOF
S + Pb $\rightarrow \pi^+\pi^+ + X$	0.59 ± 0.03	3.90 ± 0.14	24/25
S + Pb $\rightarrow \pi^-\pi^- + X$	0.62 ± 0.03	3.64 ± 0.18	15/25
p + Pb $\rightarrow \pi^+\pi^+ + X$	0.41 ± 0.03	2.35 ± 0.23	23/25

Table 4: Result of Gaussian parametrizations in $Q_{R=\tau}$

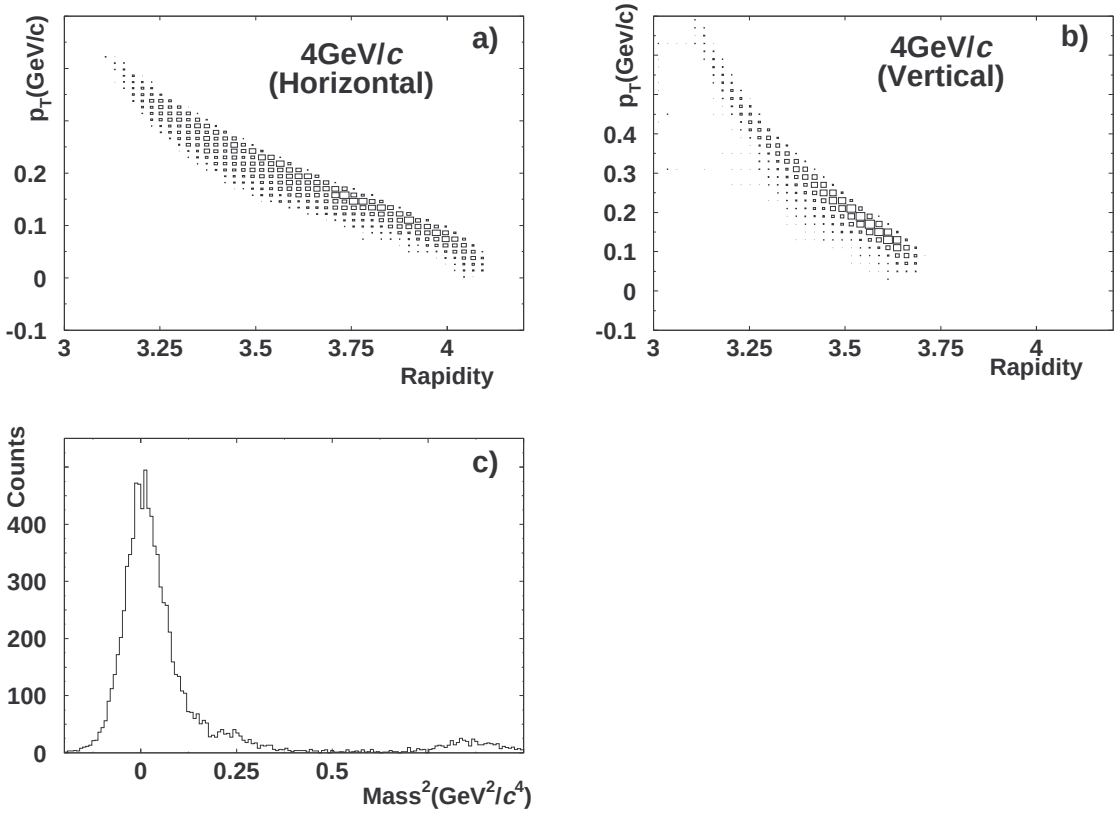

Figure 1: The NA44 acceptance and the measured mass squared as determined from the momentum and time of flight.

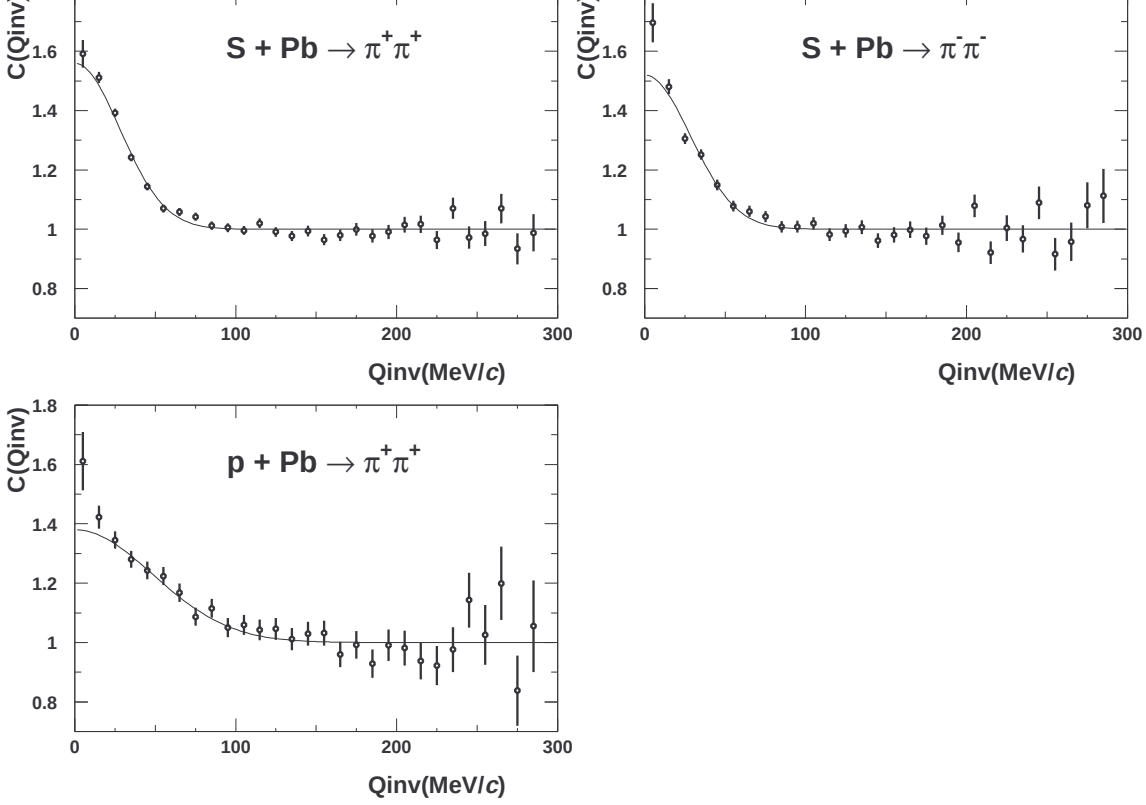

Figure 2: The Q_{inv} plots from the horizontal setting of S + Pb and p + Pb interactions.

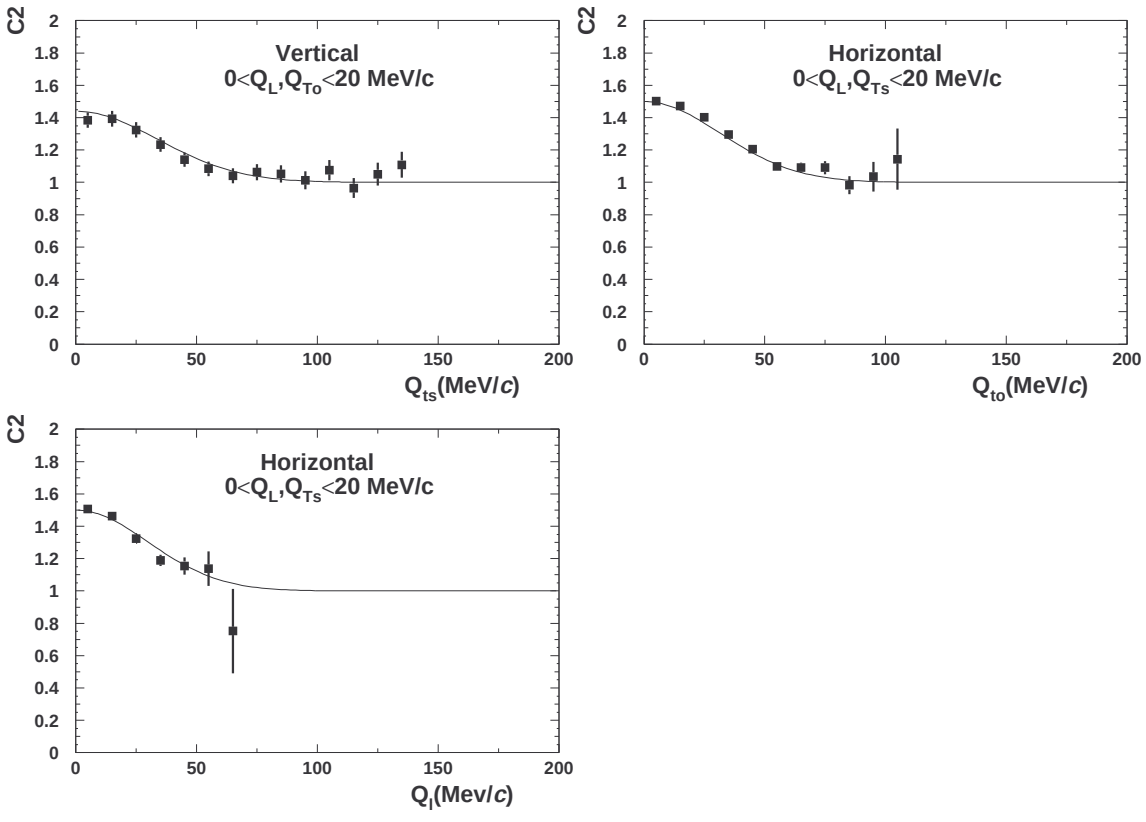

Figure 3: The Q_{t_s}, Q_{t_o} and Q_l projections. The lines represent a Gaussian fit to the data points. Error bars are statistical only.

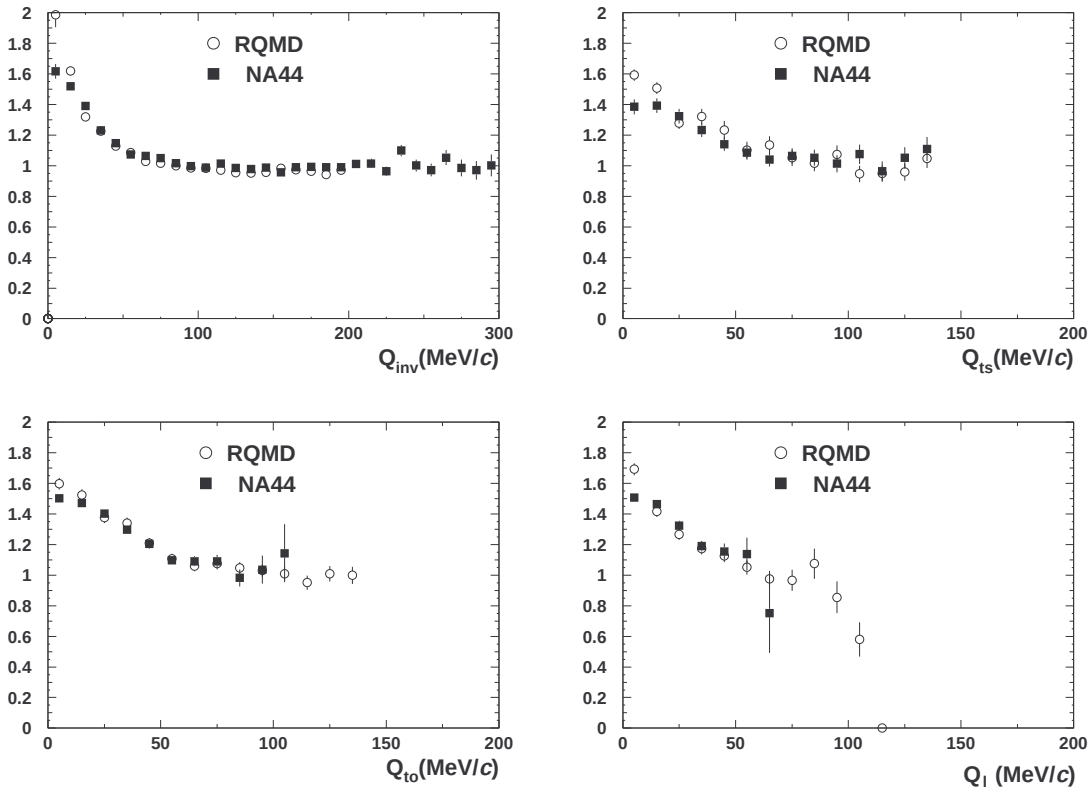

Figure 4: Comparisons of data with RQMD of the correlation function for S + Pb interactions.